ARCHIVES OF CIVIL ENGINEERING, LVIII, 1, 2012

DOI: 10.2478/v.10169-012-0004-1

ANN-BASED MODELLING OF FLY ASH COMPACTION CURVE

K. ZABIELSKA-ADAMSKA[1], M.J. SULEWSKA[2]

The use of fly ash as a material for earth structures involves its proper compaction. Fly ash compaction tests have to be conducted on separately prepared virgin samples because spherical ash grains are crushed during compaction, so the laboratory compaction procedure is time-consuming and laborious. The aim of the study was to determine the neural models for prediction of fly ash compaction curve shapes. The attempt of applying the artificial neural networks type MLP was made. ANN inputs were new-created variables – principal components dependent on grain-size distribution (as D_{10}–D_{90} and uniformity and curvature coefficients), compaction method, and fly ash specific density. The output vectors were presented by co-ordinates of generated compaction curve points. Each point (w_i, ρ_{di}) was described by two independent ANNs. Using ANN-based modelling method, models which enable establishing the approximate compaction curve shape were obtained.

Key words: Compaction curve, fly ash, fly ash compactibility, compaction parameters, geotechnical parameters, artificial neural networks, neural modelling.

1. Introduction

Soil compactibility is defined as an ability to obtain maximum possible dry density of solid particles, ρ_d, and is dependent on compaction energy, the way that is used, as well as the type of soil and its water content. Soil compaction is measured by the degree of compaction I_s:

$$I_s = \frac{\rho_d}{\rho_{d\,max}} \tag{1.1}$$

where ρ_d is the dry density of solid particles determined for soil compacted in an earth structure, $\rho_{d\,max}$ the maximum dry density of solid particles determined in the laboratory for the same material as ρ_d. Laboratory compaction test requires us to carry out compaction in standardized ways at various water contents and as a result of that plotting the relationship between dry density of solid particles (or unit weight) and

[1] PhD, DSc, Eng, Univ. Professor, Faculty of Civil and Environmental Engineering, Bialystok University of Technology, Bialystok, Poland, e-mail: kadamska@pb.edu.pl (corresponding author)

[2] PhD, DSc, Eng, Faculty of Civil and Environmental Engineering, Bialystok University of Technology, Bialystok, Poland, e-mail: m.sulewska@pb.edu.pl

water content. The moisture content at which compacted soil reaches the maximum dry density of solid particles is called optimum water content, w_{opt}. Compaction curves $\rho_d(w)$, which are obtained at various values of compaction energy, run asymptotically to the line of maximum compaction, called the zero air voids line, calculated assuming that soil pores are completely filled with water, as well as the line of saturation degree $S_r = 1$, which determines the degree of saturation when the soil sample is completely saturated.

The use of fly ash as a material for earth structures involves its proper compaction. Compaction is the most common method of the mechanical improvement of soil condition. It increases soil density, improves its strength and penetration resistance, as well as decreases compressibility and permeability. In engineering practice materials built-in road subgrade and embankment have their own specifications, which are dependent on type of earth structure and soil plasticity characteristics. Construction of mineral sealing layers usually requires cohesive soil compaction to obtain 90 or 95% of maximum compaction, relating to the Standard or Modified Proctor methods. Concern should be taken not to use degree of compaction, I_s, as the only parameter to assess compaction of material in a sealing layer or road structure. The permeability and mechanical properties of compacted cohesive soils are dependent on water content during compaction, as are properties of fly ash. Consequently, different values of geotechnical parameters are obtained for water content, w, on either side of the optimum water content, w_{opt}, on the compaction curve, for the same dry densities, ρ_d. This applies to both cohesive soil and fly ash [1]. It explains, not only a great importance of compaction parameters, but also compaction curve shape, so establishing fly ash compaction curves as density–water content relationships is very important. Additionally, fly ash compaction tests have to be conducted on separately prepared virgin samples – each point of fly ash compaction curve (w, ρ_d) should be compacted once only in a Proctor's mould. Fly ash samples compacted many times can not be considered as representative – values for maximum dry density of solid particles increase with number of repeated compaction at decreasing optimum water contents, in comparison with samples compacted only once under the same conditions. Spherical ash grains, crushed during compaction, can be stuffed with smaller grains, which improve their packing [2]. This phenomenon motivates a necessity of determination of fly ash compaction curve on virgin samples, so the procedure is time-consuming and laborious.

The paper aim is to analyse the influence of fly ash grain-size distribution (representing by the effective sizes and curvature coefficients) and specific density on its compaction parameter values, and to determine the relationship between physical parameters of tested fly ash and its compaction curve shapes. The attempt of using the artificial neural networks type Multi-Layer Perceptron (MLP) for fly ash compaction curve points was made. Results enable us to predict the shape of the tested fly ash compaction curve. Consequently, on the basis of size-grain distribution and specific density of fly ash the compaction curve shape can be modeled.

2. TESTED FLY ASH PARAMETERS

Tests were performed on a fly ash and bottom ash mixture from a dry storage yard, which are referred to as *fly ash* because there is only a vestige of bottom ash in the mix. Fly ash is a by-product of hard coal combustion at the Bialystok Thermal-Electric Power Station. The scheme of carried out laboratory tests, which results are taken into analysis, is shown in Fig. 1.

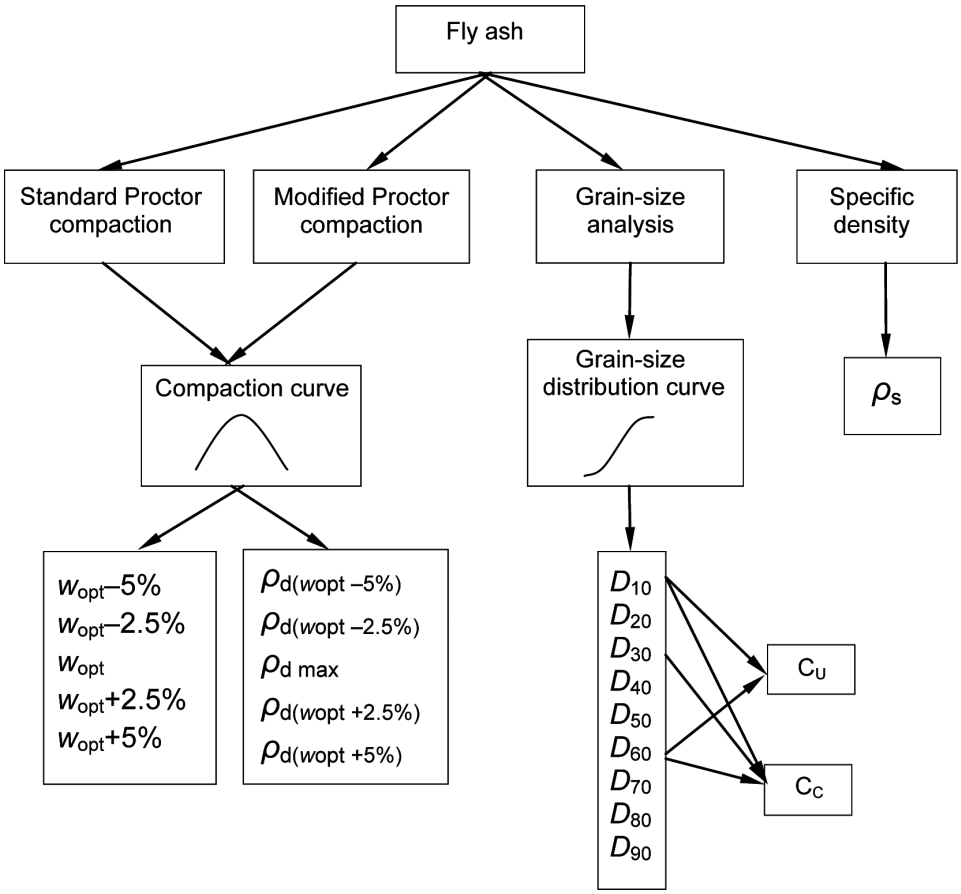

Fig. 1. Scheme of tests carried out on fly ash samples.
Rys. 1. Schemat badań przeprowadzonych na próbkach popiołu lotnego

The grain-size distribution of the tested Class F fly ash (according to ASTM C618) in most cases corresponds to sandy silt, except same cases of silty sand. On the whole, according to the criterion that mineral soils are estimated by their uniformity, C_U, and curvature, C_C, coefficients the tested fly ash qualifies as a material that responds poorly

to compaction [3]. Table 1 presents ranges of fly ash specific density and graining values.

Table 1

Tested fly ash parameters.
Parametry badanego popiołu lotnego

Parameter	Unit	Range
ρ_s	Mg/m^3	2.08–2.29
D_{10}	mm	0.009–0.025
D_{20}	mm	0.013–0.045
D_{30}	mm	0.015–0.060
D_{40}	mm	0.018–0.550
D_{50}	mm	0.022–0.500
D_{60}	mm	0.028–0.117
D_{70}	mm	0.040–0.156
D_{80}	mm	0.065–0.204
D_{90}	mm	0.105–0.500
C_U	–	2.00–6.11
C_C	–	0.80–1.73

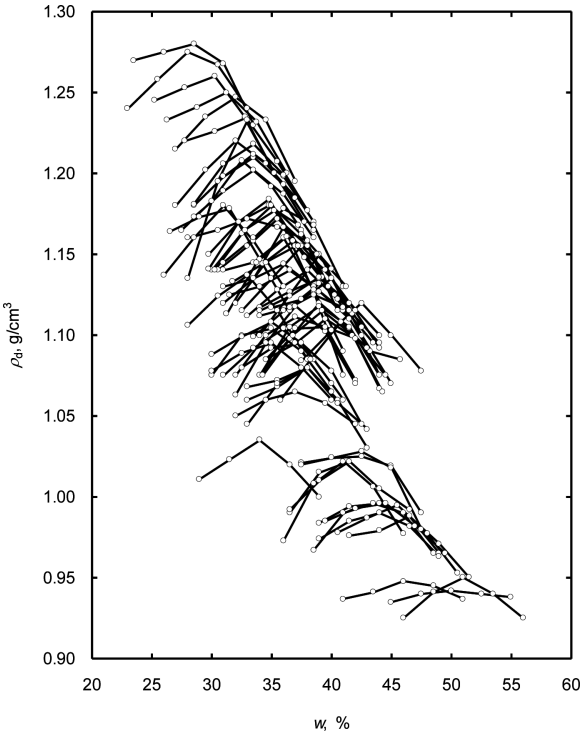

Fig. 2. The compaction curves from laboratory tests.
Rys. 2. Krzywe zagęszczalności z badań laboratoryjnych

Compaction tests were carried out by means of the Standard and Modified Proctor methods. During the tests, fly ash samples were compacted once only in a Proctor's mould – each point of compaction curve (w, ρ_d) was determined for separately prepared virgin sample [2]. Samples were moisturized so as to produce an increase in water content of each subsequent specimen of about 2% and were then stored for 24 h in closed tins. Fragmentary curves were taken into consideration for water contents ranging over w_{opt}±5% that are shown in Fig. 2.

3. ANNs IN SOIL COMPACTION

There is no many examples of neural-biased modelling of the soil compaction curve shape or even compaction parameters, w_{opt} and ρ_{dmax}, in literature.

One of the first attempt of applying ANNs to prediction values of w_{opt} and ρ_{dmax} (as two outputs) for the synthetic and natural cohesive soils was made by Najjar et al. [4] on the basis of graining (soil composition percentages), specific density, as well as consistency parameters: liquid and plastic limits. Fineness modulus, uniformity coefficient and effective sizes, D_{50} and D_{10}, were recognized as less significant. It should be stated that calculations were based on data available in the literature and only compaction parameters, w_{opt} and ρ_{dmax}, were complemented in laboratory due to the limited data available, so computation results could be less accurate.

Similar research was presented in [5, 6]. The first analysis of Sinha and Wang [5] was performed for five input variables: specific density, fineness modulus, effective size, D_{10}, plastic and liquid limits, and the only one output – maximum dry density of solid particles. The second one [5] was carried out for three inputs: fineness modulus, coefficient of uniformity and plastic limit for optimum water content prediction. Next, the combined model was considered, where both compaction parameters, w_{opt} and ρ_{dmax}, were predicted together with coefficient of permeability. All three models could become an efficient tool useful in earth works. In Günaydın's analysis [6], including five different models, the number of inputs changed from seven to two was employed. The inputs were: contents of particular soil fraction (fine-grained, sand, gravel), specific density, liquid and plastic limits and soil type (the soil name). Compaction parameters, w_{opt} and ρ_{dmax}, were both applied as outputs. All of the models were discussed in detail.

The compaction parameters, w_{opt} and ρ_{dmax}, or minimum and maximum dry densities determined by vibration of dry soil, ρ_{dmin} and ρ_{dmax}, were found for non-cohesive soils in dependence on soil graining (coefficient of uniformity and effective sizes: D_{10}–D_{90}) by Sulewska [7, 8, 9]. Principal Component Analysis was also used to decrease the ANN size through input data compression. As outputs were applied: w_{opt}, ρ_{dmax}, and determined by vibration: ρ_{dmax} and ρ_{dmin}, separately or in combination.

In all the mentioned cases only one dynamic compaction method was considered – the Standard Proctor test.

The shape of compaction curve was only predicted by Basheer [10] for cohesive soils, depending on soil graining (fines content, clay content), specific density, consistency parameters: liquid and plastic limits, and compaction energy (reduced, the Standard and Modified Proctor energy). The research was developed for determining compaction curves in two stages: optimum water content from one model and dry density of solid particles from another. The density models were found to be significantly more accurate, so actual values of w_{opt} were used in curve simulations.

Authors made an attempt of applying the ANNs for fly ash compaction curve shape for standard and modified compaction methods, which was described briefly in [11].

4. ANN-based modelling technique

Analysed data set of a total of 71 compaction curves (P=71 cases) was described by means of 22 variables (Fig. 1):

- compaction method (standard or modified);
- co-ordinates of points on compaction curves (w_i, ρ_{di}) where w_i is: $w_{opt}-5\%$, $w_{opt}-2.5\%$, w_{opt}, $w_{opt}+2.5\%$, $w_{opt}+5\%$, and ρ_{di} is: $\rho_{d(wopt-5\%)}$, $\rho_{d(wopt-2.5\%)}$, ρ_{dmax}, $\rho_{d(wopt+2.5\%)}$, $\rho_{d(wopt+5\%)}$;
- specific density, ρ_s;
- grain-size distribution described by effective sizes: D_{10}, D_{20}, D_{30}, D_{40}, D_{50}, D_{60}, D_{70}, D_{80}, D_{90} and uniformity and curvature coefficients, C_U and C_C.

In order to perform the data set compression to reduce the size of the network with a large number of parameters Principal Component Analysis (PCA) was used [12, 13]. PCA reduces the dimensionality of the data set, while retaining a variance by mapping the co-ordinate system described by actual variables to a new lower dimensional co-ordinate system specified by principal components. PCA lies in the fact of redistribution of variance over new-created variables that can explain, when all the principal components are considered, 100% of the total variance. Each new-created variable (the principal component, PC) is a linear combination of the actual variables. Contribution of the particular variables to element of PC is determined by loadings of each original variable on the appropriate PC. In the paper the PCs are a result of original set of 13 data: compaction method, ρ_s, $D_{10} - D_{90}$, C_U, C_C. The PCs are orthogonal (that is uncorrelated) linear combinations of the original variables. *STATISTICA* software was used for calculating the principal components by means of the factor analysis function.

Table 2 presents the percentage of variance that is explained by each of principal components. The first principal component, PC1, accounts for 41.46% of the total variance; the second (PC2) and third (PC3) principal components account for 25.28% and 10.57% of the total variance respectively; the fourth (PC4) and fifth (PC5) principal components account for 8.40% and 7.40% of the total variance respectively; the sixth (PC6) accounts for 4.24%.

Table 2

Analysis of principal components.
Analiza składowych głównych

PCs	% Total Variance	Cumulative %
PC1	41.46	41.46
PC2	25.28	66.74
PC3	10.57	77.31
PC4	8.40	85.71
PC5	7.10	92.81
PC6	4.24	97.05
PC7	1.83	98.88
PC8	0.71	99.59
PC9	0.29	99.88
PC10	0.08	99.96
PC11	0.02	99.98
PC12	0.01	99.99
PC13	0.01	100.00

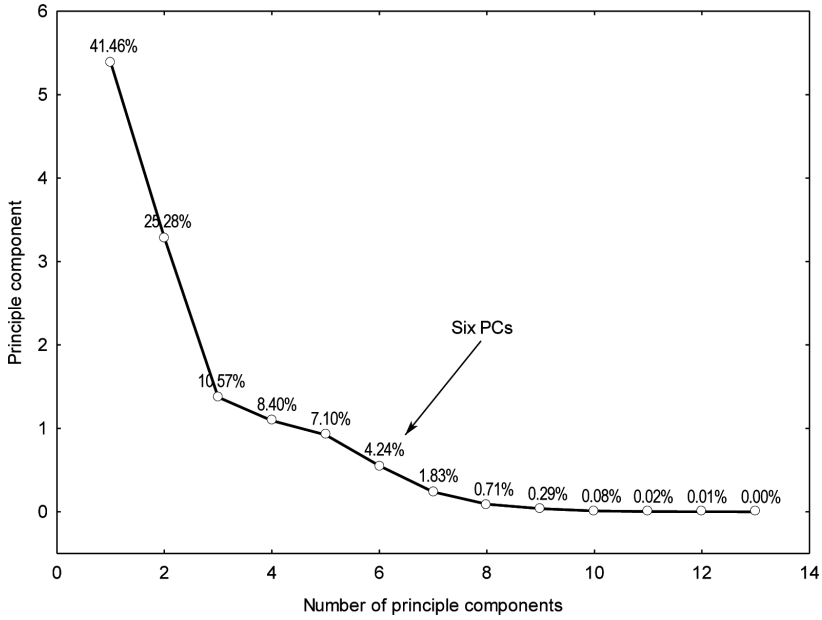

Fig. 3. Percentage of variance explained by following PCs.
Rys. 3. Procent wariancji określony przez kolejne składowe główne

A number of principal components taken into further analysis was establish on the basis of Cattell's criterion [14] (Fig. 3). It was necessary to establish the points

on the left of the straight line on the graph presenting percentage of variance that was explained by following PCs (or eigenvalues). Such a point is determined by initial six PCs, which explained 97.05% of the total variance, at a loss of 2.95% of the information. In accordance with this criterion it is sufficient to use only six PCs.

Table 3 shows the loadings of each original variable on the corresponding principal component. These loadings describe correlations between the particular original variables and the PCs. It can state that PC1 is characterised by high loading on: ρ_s, D_{60}–D_{90} and C_U. PC2 is characterised by high loading on variables: D_{10}–D_{30} and C_C; PC3 – by D_{40}; PC4 – by D_{50}; PC5 – by variable: compaction method. PC6 is not characterised by any dominant loading.

Table 3

Loadings for PC1–PC6.
Ładunki czynnikowe zmiennych dla PC1–PC6

Variable	PC1	PC2	PC3	PC4	PC5	PC6
Method	0.091	–0.035	0.363	–0.505	0.765	0.134
ρ_s	–0.739	0.286	–0.111	0.268	0.060	0.521
D_{10}	0.158	–0.849	–0.382	–0.127	–0.038	0.257
D_{20}	0.446	–0.796	–0.220	–0.183	–0.065	–0.025
D_{30}	–0.375	–0.919	0.042	0.047	0.013	–0.017
D_{40}	0.347	–0.276	0.744	0.398	–0.112	0.241
D_{50}	0.150	–0.098	–0.447	0.660	0.550	–0.163
D_{60}	–0.897	–0.357	0.073	0.021	–0.000	–0.062
D_{70}	–0.987	–0.117	–0.030	0.049	0.027	0.074
D_{80}	–0.967	–0.181	–0.085	0.008	0.058	–0.018
D_{90}	–0.893	–0.319	0.032	–0.208	–0.063	–0.099
C_U	–0.858	0.246	0.309	0.066	0.026	–0.267
C_C	0.281	–0.762	0.412	0.261	0.069	–0.140

The data set was randomly split into the learning (L), the validating (V) and the testing (T) subsets. The pattern number in particular subsets was in the ratio of 50:25:25% of the total number of patterns, respectively. Co-ordinates of points on compaction curves were modelled using multilayer feed forward neural networks (type MLP) with 6 or 5 inputs, one hidden layer and one output. In neurons of the hidden layer the tangensoidal (tanh) activation function was applied, and in the output neurons – the linear activation function. The Levenberg-Marquardt method was used for neuron networks training. ANN simulation was performed using *STATISTICA Neural Networks* software. ANNs with the best prediction accuracy were quantified by the means of the various error measure analysis. In the paper both the root mean squared error, *RMSE* and the determination coefficient, R^2, independently for L, V, and T subsets were

shown:

$$RMSE = \sqrt{\frac{1}{\mathrm{P}} \sum_{i=1}^{\mathrm{P}} \left(d_{\mathrm{i}} - y_{\mathrm{i}}\right)^2} \tag{4.1}$$

$$R^2 = 1 - \frac{\sum (d_{\mathrm{i}} - y_{\mathrm{i}})^2}{\sum \left(d_{\mathrm{i}} - \bar{d}\right)^2} \tag{4.2}$$

where d_{i} are the measured values, y_{i} are the predicted values of d_{i}, and $\bar{d}$ is the mean of the d_{i} values. ANNs with the best prediction accuracy along with values of error measures are shown in Table 4.

Table 4

ANNs of the best prediction accuracy and their error measures.
SNN o najlepszej dokładności predykcji i ich miary błędów

Output	Inputs	ANN	Epochs	*RMSE*			R^2		
				L	*V*	*T*	*L*	*V*	*T*
$w_{\mathrm{opt}}-5\%$	PC1–PC6	6-2-1	324	0.130	0.094	0.122	0.615	0.697	0.579
$w_{\mathrm{opt}}-2.5\%$	PC1–PC6	6-4-1	264	0.055	0.091	0.117	0.933	0.823	0.709
w_{opt}	PC1–PC6	6-3-1	787	0.057	0.122	0.123	0.925	0.671	0.743
$w_{\mathrm{opt}}+2.5\%$	PC1–PC6	6-4-1	184	0.112	0.136	0.125	0.697	0.575	0.564
$w_{\mathrm{opt}}+5\%$	PC1–PC6	6-3-1	289	0.117	0.109	0.167	0.632	0.557	0.584
$\rho_{\mathrm{d(wopt-5\%)}}$	PC1–PC5	5-3-1	101	0.051	0.083	0.080	0.929	0.903	0.741
$\rho_{\mathrm{d(wopt-2.5\%)}}$	PC1–PC2, PC4–PC6	5-3-1	517	0.077	0.088	0.100	0.880	0.878	0.906
ρ_{dmax}	PC1–PC2, PC4–PC6	5-3-1	117	0.053	0.100	0.096	0.949	0.839	0.867
$\rho_{\mathrm{d(wopt+2.5\%)}}$	PC1–PC6	6-3-1	138	0.064	0.094	0.079	0.927	0.837	0.874
$\rho_{\mathrm{d(wopt+5\%)}}$	PC1–PC6	6-3-1	993	0.075	0.087	0.083	0.867	0.916	0.914

Figures 4a and b present the exemplary comparison of the measured values and the predicted ones with ANNs in the set of all data, along with relative error areas

$$RE = \left| \frac{y_{\mathrm{i}} - d_{\mathrm{i}}}{y_{\mathrm{i}}} \right| \cdot 100\% \tag{4.3}$$

respectively for w_{opt} and ρ_{dmax}. Exemplary compaction curves predicted by ANNs compared with actual fly ash compaction curves are presented in Figure 5.

5. Summary and conclusions

The aim of the study was to determine the neural models for prediction of fly ash compaction curve shapes characterised by co-ordinates of five points on the basis of

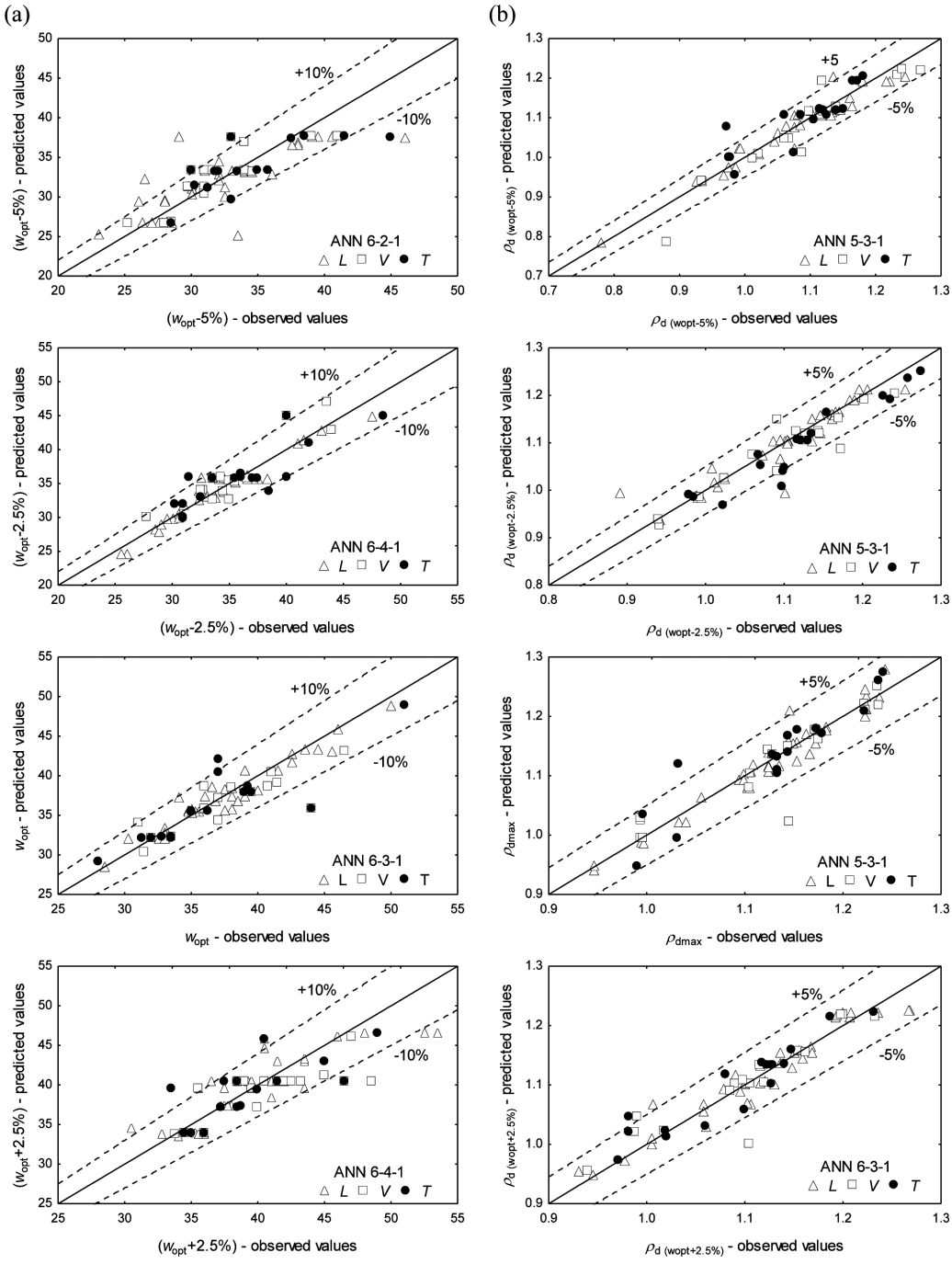
(a)
(b)
+10%
-10%
+5
-5%
+5%
ANN 6-2-1
ANN 5-3-1
ANN 6-4-1
ANN 6-3-1
L V T
(wopt-5%) - predicted values
(wopt-5%) - observed values
ρd (wopt-5%) - predicted values
ρd (wopt-5%) - observed values
(wopt-2.5%) - predicted values
(wopt-2.5%) - observed values
ρd (wopt-2.5%) - predicted values
ρd (wopt-2.5%) - observed values
wopt - predicted values
wopt - observed values
ρdmax - predicted values
ρdmax - observed values
(wopt+2.5%) - predicted values
(wopt+2.5%) - observed values
ρd (wopt+2.5%) - predicted values
ρd (wopt+2.5%) - observed values

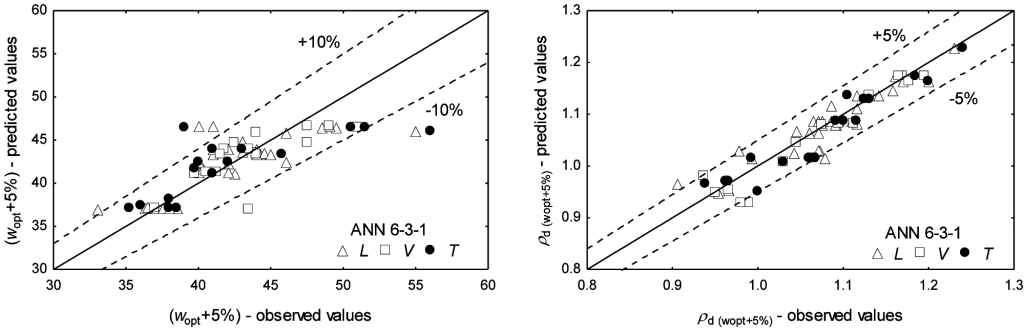

Fig. 4. Values obtained from laboratory tests and calculated by ANNs in all data set: (a) w_i values along with 10% relative errors areas, (b) ρ_{di} values along with 5% relative errors areas.
Rys. 4. Wartości otrzymane z badań laboratoryjnych i obliczone przez SSN w całym zbiorze danych: (a) wartości w_i z obszarem 10% błędu względnego, (b) wartości ρ_{di} z obszarem 5% błędu względnego

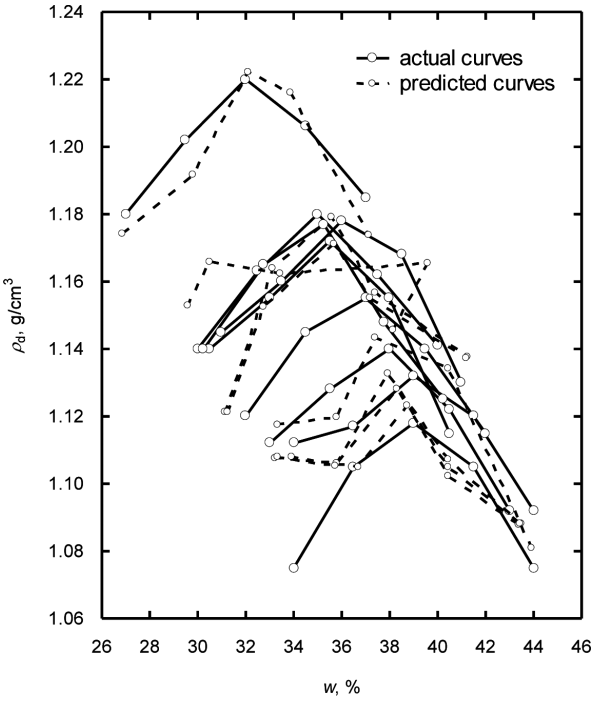

Fig. 5. Exemplary actual and predicted by ANNs compaction curves.
Rys. 5. Przykładowe rzeczywiste i przewidywane za pomocą SSN krzywe zagęszczalności

grain-size distribution and specific density. Each point (w_i, ρ_{di}) was described by two independent ANNs. ANN inputs were new-created variables – principal components PCs, and outputs were co-ordinates of the compaction curve points. PCs are a result of: compaction method, ρ_s, $D_{10} - D_{90}$, C_U, C_C.

The neural networks of various topology: 6-3-1, 6-2-1 and 6-4-1 for moisture, w_i, predicted values, and 5-3-1 and 6-3-1 for dry density of solid particles, ρ_{di}, values proved to be the best. The obtained neural networks have a satisfactory prediction quality, especially for ρ_{di} values. The determination coefficient, R^2, between the measured values of point co-ordinate and the predicted ones is in the range 0.557–0.823 in the validating subset and 0.564–0.743 in the testing subset, and 0.837–0.916 in the validating subset and 0.867–0.914 in the testing subset, respectively for w_i and ρ_{di} values. Water content at compaction decreases accuracy of the predicted compaction curve shapes, especially for w_i greater than optimum water content.

Using ANN-based modelling method, models which enable establishing the approximate compaction curve shape were obtained.

REFERENCES

1. K. ZABIELSKA-ADAMSKA, *Fly ash as a material for constructing sealing layers* [in Polish], Publishing House of Bialystok University of Technology, Bialystok 2006.
2. K. ZABIELSKA-ADAMSKA, *Laboratory compaction of fly ash and fly ash with cement addition*, Journal of Hazardous Material, **151**, 2-3, 48-489, 2008.
3. K. ZABIELSKA-ADAMSKA, *Shear strength parameters of compacted fly ash–HDPE geomembrane interfaces*, Geotextiles & Geomembranes, **24**, 2, 91-102, 2006.
4. Y.M. NAJJAR, I.A. BASHEER, W.A. NAOUSS, *On the identification of compaction parameters by neuronets*, Computers & Geotechnics, **18**, 3, 167-187, 1996.
5. S.K. SINHA, M.C. WANG, *Artificial neural network prediction models for soil compaction and permeability*, Geotechnical and Geological Engineering, **26**, 1, 47-64, 2008.
6. O. GÜNAYDIN, *Estimation of soil compaction parameters by using statistical analyses and artificial neural networks*, Environmental Geology, **57**, 1, 203-215, 2009.
7. M.J. SULEWSKA, *Artificial neural networks in the evaluation on non-cohesive soil compaction parameters* [in Polish], Institute of Fundamental Technological Research Polish Academy of Sciences, Warsaw-Bialystok 2009.
8. M.J. SULEWSKA, *Neural modelling of compactibility characteristics of cohesionless soil*, Computer Assisted Mechanics and Engineering Sciences, **17**, 1, 27-40, 2010.
9. M.J. SULEWSKA, *Prediction models for minimum and maximum dry density of non-cohesive soils*, Polish Journal of Environmental Studies, **19**, 4, 797-804, 2010.
10. I.A. BASHEER, *Empirical modeling of the compaction curve of cohesive soils*, Canadian Geotechnical Journal, **38**, 1, 29-45, 2001.
11. K. ZABIELSKA-ADAMSKA, M.J. SULEWSKA, *Neural modelling of the fly ash compaction curve*, Proc. 15 European Conf. on Soil Mechanics and Geotechnical Engineering, 601-606, Athens 2011.
12. M. JAMBU, *Exploratory and Multivariate Data Analysis*, Academic Press, New York 1991.
13. S. HAYKIN, *Neural Networks: A Comprehensive Foundation*, 2nd Edition, NJ: Prentice Hall, Englewood Cliffs 1999.
14. R.B. CATTELL, *The scree test for the number of factor*, Multivariate Behavioural Research, **1**, 245-276, 1966.

MODELOWANIE KRZYWEJ ZAGĘSZCZALNOŚCI POPIOŁU LOTNEGO ZA POMOCĄ SSN

Streszczenie

Wykorzystanie popiołu lotnego do konstrukcji ziemnych wymaga jego właściwego zagęszczenia. Zagęszczanie powoduje wzrost gęstości gruntu, zwiększa jego wytrzymałość i zdolność do przenoszenia obciążeń, a także zmniejsza ściśliwość i przepuszczalność. Oznaczenie zagęszczalności popiołu lotnego musi być przeprowadzane na próbkach jednokrotnie zagęszczanych, ponieważ sferyczne ziarna popiołu są niszczone w trakcie ubijania, w związku z tym, laboratoryjne ustalenie krzywej zagęszczalności popiołu jest bardzo czasochłonne. Celem artykułu było wykorzystanie modelowania neuronowego do prognozy kształtu krzywej zagęszczalności popiołu lotnego. Podjęto próbę zastosowania sztucznych sieci neuronowych SSN typu MLP do opisu punktów krzywej zagęszczalności. Każdy punkt krzywej (w_i, ρ_{di}) został opisany przez dwie niezależne SSN. Wykorzystano SSN o różnych wejściach, którymi były nowo utworzone zmienne – składowe główne, zależne od uziarnienia (średnic efektywnych d_{10}–d_{90} oraz wskaźników jednorodności i krzywizny uziarnienia), metody zagęszczenia oraz gęstości właściwej szkieletu gruntowego. Wektorami wyjścia były współrzędne punktów krzywej zagęszczalności popiołu lotnego. Najlepszymi sieciami neuronowymi były sieci o topologii: 6-3-1, 6-2-1 i 6-4-1 dla prognozy wartości wilgotności w_i, oraz 5-3-1 i 6-3-1 dla predykcji wartości gęstości objętościowej szkieletu gruntowego ρ_{di}. Uzyskano sieci neuronowe o zadowalającej precyzji, szczególnie w przypadku wartości ρ_{di}. Modelowanie krzywej za pomocą SSN umożliwiło ustalenie przybliżonego kształtu krzywej zagęszczalności popiołu lotnego.

Remarks on the paper should be sent to the Editorial Office no later than June 30, 2012

Received October 29, 2011
revised version
February 25, 2012